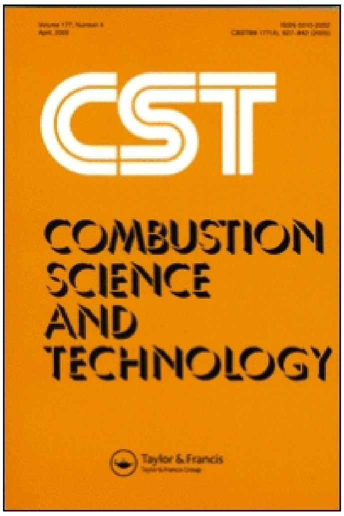

Combustion Science and Technology
Publication details, including instructions for authors and subscription information:
http://www.informaworld.com/smpp/title~content=t713456315

Transient Combustion Response of AP/HTPB Composite Propellant to Acoustic Oscillations in a Rocket Motor

Weidong Cai [a]; Piyush Thakre [a]; Vigor Yang [a]
[a] Department of Mechanical and Nuclear Engineering, The Pennsylvania State University, University Park, Pennsylvania, USA

Online Publication Date: 01 April 2009

To cite this Article Cai, Weidong, Thakre, Piyush and Yang, Vigor(2009)'Transient Combustion Response of AP/HTPB Composite Propellant to Acoustic Oscillations in a Rocket Motor',Combustion Science and Technology,181:4,597 — 617

To link to this Article: DOI: 10.1080/00102200802693781

URL: http://dx.doi.org/10.1080/00102200802693781

Combust. Sci. and Tech., 181: 597–617, 2009

ISSN: 0010-2202 print/1563-521X online
DOI: 10.1080/00102200802693781

TRANSIENT COMBUSTION RESPONSE OF AP/HTPB COMPOSITE PROPELLANT TO ACOUSTIC OSCILLATIONS IN A ROCKET MOTOR

Weidong Cai, Piyush Thakre, and Vigor Yang
Department of Mechanical and Nuclear Engineering, The Pennsylvania State University, University Park, Pennsylvania, USA

A comprehensive theoretical/numerical model is developed to investigate the transient combustion response of AP/HTPB composite propellant to acoustic excitation in a rocket-motor environment. The work extends our previous analysis of AP/HTPB combustion at steady-state to include flow oscillations and their subsequent influence on the flame structure and propellant burning behavior. Detailed information about the flame-zone physiochemistry near the propellant surface is obtained at different locations in the motor for the first three modes of longitudinal acoustic waves. In addition, various mechanisms dictating the characteristics of the propellant combustion response, including microscale motions in the flame zone and macroscale motions in the bulk flow, are explored. The effects of mean and oscillatory flowfields in determining the propellant combustion response are also examined. Furthermore, a large flow velocity fluctuation often leads to a nonlinear response of the heat feedback to the propellant surface and the resultant burning rate.

Keywords: AP/HTBP composite propellant; Combustion instability; Solid rocket motor; Transient combustion

INTRODUCTION

Combustion instability in solid-propellant rocket motors results from interactions between acoustic waves and unsteady combustion processes in the chamber. For ammonium perchlorate (AP)-based composite propellants, acoustic flow oscillations affect propellant burning characteristics not only by influencing reaction kinetics, but also by altering the local mixing of fuel and oxidizer and the ensuing diffusion flame structure in the gas phase. This in turn produces acoustic disturbances by means of unsteady mass, momentum, and energy additions from the burning propellant into the gas stream. A mutual coupling can thus occur between the oscillatory flowfield and the transient combustion response of the propellant. The resultant pressure fluctuations may reach sufficient amplitudes to interfere adversely with the desired motor operation (Culick & Yang, 1992).

Received 26 June 2008; revised 24 November 2008; accepted 5 December 2008.
This work was sponsored partly by the Pennsylvania State University and partly by the California Institute of Technology Multidisciplinary University Research Initiative under ONR grant number N00014-95-1-1338, Program Manager Dr. Judah Goldwasser.
Address correspondence to Vigor Yang, The Pennsylvania State University, 104 Research Building East, University Park, PA 16802, USA. E-mail: vigor@psu.edu

The study of transient combustion response of a propellant to incident pressure oscillation dates back to the early 1960s (Culick, 1968; Novozhilov, 1965). The obtained pressure-coupled response function was treated as a propellant property and was used to study the stability behavior of a rocket motor (Culick & Yang, 1992). Levine and Baum (Baum & Levine, 1986; Levine & Baum, 1983) conducted a nonlinear instability analysis by combining one-dimensional gas dynamics with a simple heuristic model of combustion response. Cohen and Strand (1985a, 1985b) extended the work by accounting for the propellant composition and AP particle size. Wicker et al. (1996) examined the dependence of motor stability behavior on the functional form of the combustion response function. Most existing models (Brewster & Son, 1995; Brewster et al., 2000) for solid-propellant combustion response employ the quasi-steady gas phase, homogeneous, one-dimensional (QSHOD) approximation. The change in the flame structure and associated heat release due to acoustic oscillations is generally not considered. In spite of their contributions to the understanding of combustion instability, these models provide limited information concerning the burning behavior of composite propellants amid the oscillatory crossflows typical in rocket motors. The heterogeneous effects inherent to the combustion of composite propellants are also not taken into account. Furthermore, the notion that the multi-modal AP particle distribution is responsible for a multi-peaked response function has not been accepted. A comprehensive analysis encompassing a multi-dimensional flame structure in a rocket-motor environment is thus needed to improve the knowledge of the combustion response of AP/HTPB propellant to acoustic oscillations.

The transient response of premixed flames to acoustic waves in a porous-walled chamber has been addressed by Chu et al. (2003). This paper focuses on diffusion flames and extends our earlier work (Cai et al., 2008) on steady combustion of AP/HTPB composite propellant. The previous analysis investigated the effects of chamber pressure, local flowfield, and AP mass fraction and particle size on the propellant flame structure and burning characteristics in a rocket-motor environment. The current focus is placed on the transient response to acoustic oscillations in the chamber. The formulation includes conservation equations in both the gas and condensed phases, and accommodates finite-rate chemical kinetics and variable thermophysical properties. The gas- and condensed-phase processes are matched at the interface to determine the instantaneous propellant burning behavior. Only laminar flows are considered here, to avoid complications arising from turbulence. Detailed flame structures and heat-release distributions at various axial locations, including microscale motions in the flame zone and macroscale motions in the bulk flow, are analyzed in a systematic manner.

In the following section, the theoretical formulation and numerical method are briefly described. The analysis starts with calculations of the motor internal flowfields and propellant burning behavior under steady operating conditions. Subsequently, periodic pressure oscillations are imposed at the exit to simulate standing acoustic waves in the chamber. The interactions between the unsteady combustion process and oscillatory flows, as well as their influence on the motor instability, are investigated thereafter.

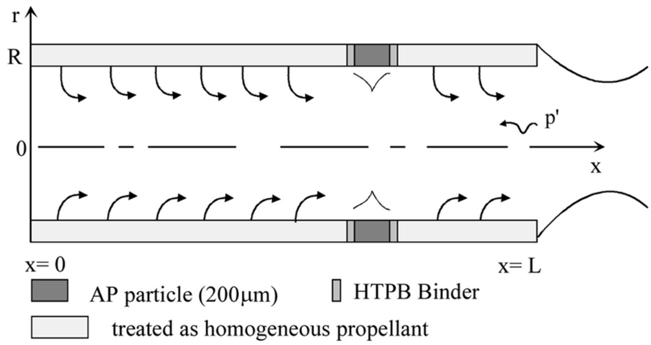

Figure 1 Schematic diagram of a rocket motor loaded with AP/HTPB propellant.

THEORETICAL FORMULATION AND NUMERICAL SCHEME

The physical model considered is shown schematically in Figure 1. It consists of a cylindrical chamber loaded with AP/HTPB composite propellant and an exhaust nozzle. A sandwich-type of segment containing AP and HTPB is embedded in the propellant grain. The location of the sandwich can be varied in the motor, so that the burning properties and combustion wave structures of the propellant can be studied under different flow environments. The gas-phase formulation involves a multi-component reacting system with variable thermodynamic and transport properties. The condensed phase consists of a preheated zone and a thin superficial reaction layer in which thermal diffusion and decomposition reactions take place. The details of the conservation equations and the AP/HTPB combustion model are described in our previous work (Cai et al., 2008). A zeroth-order reaction is assumed for the condensed-phase decomposition of AP, based on the work of Guirao and Williams (1971). For gas-phase combustion, the substitution of ethylene for the HTPB pyrolysis products has been found reasonable (Cai et al., 2008).

A preconditioning technique with dual-time stepping integration is employed (Hsieh & Yang, 1997; Tseng & Yang, 1994; Zong & Yang, 2007) to solve the conservation equations numerically. The algorithm circumvents the difficulties arising from the disparity in system eigenvalues due to the low Mach-number regime and stiffness of chemical source terms. Spatial discretization is achieved with a second-order central difference scheme. The numerical framework has been verified and validated against several selected problems involving acoustic excitations (Cai et al., 2003; Flandro et al., 2000) and stiff source terms (Roh et al., 1998; Zong & Yang, 2008).

RESULTS AND DISCUSSION

Figure 1 shows the physical model of concern, an axisymmetic chamber with a closed head-end. It measures 0.5 meter in length and 4.22 cm in diameter. The overall dimensions are five-sixths those of the motor previously considered by Culick and Yang (1992). The chamber pressure is set as 70 atm. Only the upper half of the volume is treated because of the flow symmetry with respect to the centerline. The computation domain for the condensed phase is 50 μm in depth, about twice the estimated thickness of the AP preheat zone at 70 atm. The dimensions of the embedded AP/HTPB sandwich-type of segment are identical to those used in our previous study on steady-state combustion (Cai et al., 2008). The widths of the AP (d_{AP}) and HTPB (d_{HTPB}) elements are 200 and 171 μm, respectively, equivalent to a mass ratio of 7/3. Inert gases simulating the combustion products from the propellant are injected from the rest of the wall at a prescribed condition.

The steady-state flowfield was first established in the chamber to provide the initial condition (Cai et al., 2008). Periodic pressure oscillations are then imposed at the chamber exit to simulate longitudinal standing waves. The forcing frequencies are 1080, 2160, and 3240 Hz, corresponding to the first, second, and third longitudinal modes of the chamber acoustics, respectively. The amplitude of the oscillation is 2% of the mean pressure. In order to study the interaction between the gas-phase flame dynamics and the oscillating crossflow, the sandwich-type propellant segment is placed at three different locations, 3.2, 25, and 46.96 cm from the head end of the chamber. Figure 2 shows the normal acoustic pressure and velocity distributions of the first three longitudinal modes, as well as the locations of the propellant segment. Data acquisition and analysis of the unsteady flowfield were conducted after the fifteenth cycle of the imposed acoustic field, when stationary oscillations are attained.

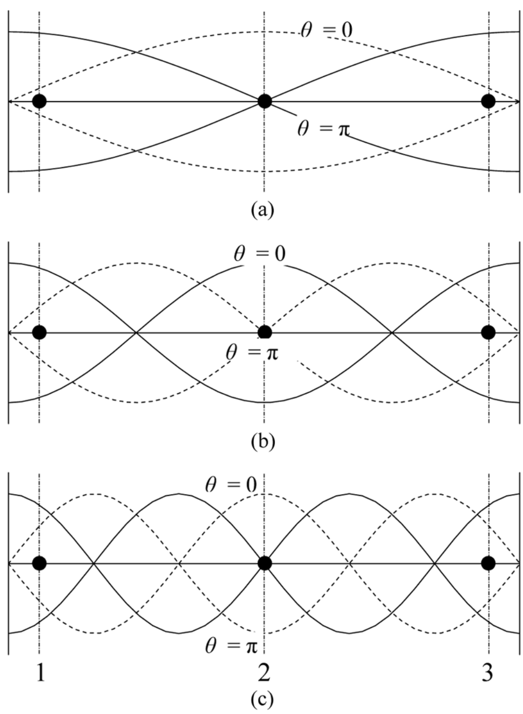

Figure 2 Distributions of acoustic velocity and pressure of (a) first, (b) second, and (c) third longitudinal modes of acoustic oscillation at phase angles of 0 and π (--- acoustic velocity, —acoustic pressure, ● location of AP/HTPB sandwich).

Acoustic Pressure and Velocity Fields

The oscillatory flowfield was examined first. Figure 3 shows the contour plots of the pressure amplitude of the first and second modes of standing acoustic waves. The low Mach-number environment renders a one-dimensional acoustic pressure field, with no discernible variation in the radial direction. The phenomenon of acoustic refraction, commonly observed for waves traveling in a nonuniform medium, is not evident here. Figure 4 shows the distributions of the amplitudes of the axial velocity fluctuations for the first two modes. The complex structure adjacent to the surface indicates the presence of an acoustic boundary layer within which rapid fluctuations arising from acoustic disturbances, unsteady shear waves, and flame oscillations occur (Apte & Yang, 2002; Flandro et al., 2000; Majdalani, 1999; Roh et al., 1998). The acoustic wave couples with the mass injection from the propellant surface and generates fluctuating vorticity to satisfy the no-slip boundary condition. The acoustic oscillations can also affect the flame dynamics and produce entropy fluctuations.

Based on the linear approximation for small amplitude oscillations, the axial velocity fluctuation u' comprises three contributions (Pierce, 1989):

$$u' = u'_a + u'_v + u'_s \tag{1}$$

where a, v, and s represent the acoustic (irrotational), vorticity (shear), and entropy (thermal) disturbances, respectively. The amplitude of the velocity fluctuation in Figure 4 reaches a maximum of 18 m/s at the acoustic pressure node, consistent with classical acoustic theory (i.e., $|u'| = |p'|/\rho a$). The velocity fluctuation in the core region is one-dimensional because the vorticity and entropy disturbances are

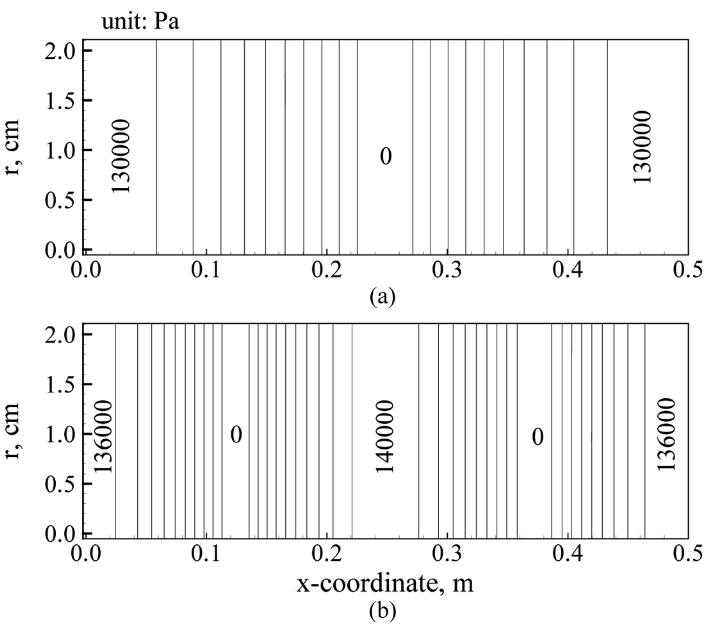

Figure 3 Distributions of amplitudes of pressure oscillations in rocket motor: (a) first mode, (b) second mode.

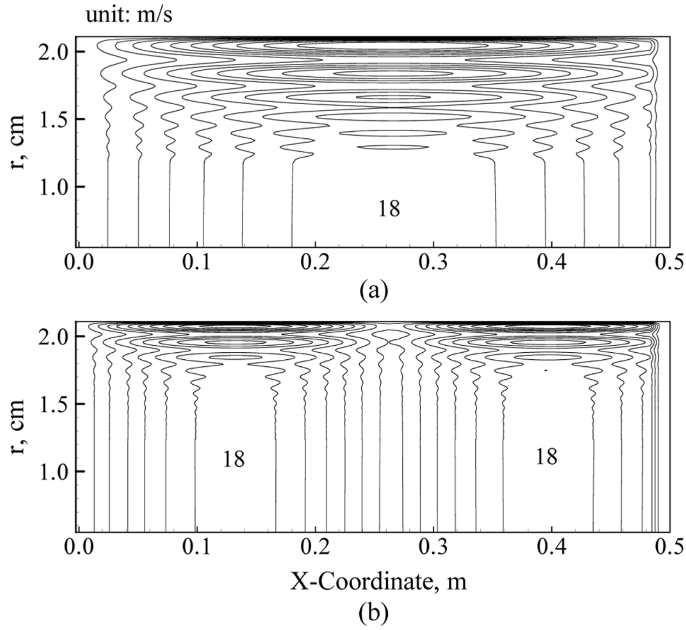

Figure 4 Distributions of amplitudes of axial-velocity fluctuations in rocket motor (a) first mode (b) second mode.

smoothed out by viscous dissipation and heat conduction, respectively. The primary difference between the two modes lies in the spatial structure and phase distribution of the oscillatory field. Because the flame zone is located very close to the burning surface, the acoustic boundary-layer thickness is primarily influenced by the shear wave. The oscillation frequency plays a key role in the viscous damping of the shear wave and thus the radial penetration of the disturbance (Flandro et al., 2000; Majdalani & Van Moorhem, 1997). Figure 4 shows that the thickness of the acoustic boundary layer decreases with increasing frequency due to enhanced viscous damping.

Entropy Waves

Figure 5 shows a close-up view of the amplitude of axial-velocity fluctuation in the flame zone for the first mode. The propellant sandwich is located at $x = 3.2$ cm. According to Pierce (1989), the contribution of the entropy component of the axial-velocity fluctuation is proportional to the fluctuation of the temperature gradient (i.e., $u' \propto (\nabla T)'$). Figure 6 shows the contour plot of $|(dT/dx)'|$, bearing a close resemblance to the distribution of $|u'_s|$. The contribution of the entropy disturbance to the velocity fluctuation in the flame zone is evident. To further quantify this phenomenon, the radial distribution of $|u'|$ in the near-surface region is examined. Figure 7a shows the radial distribution of the amplitude of the axial-velocity fluctuations at $x = 3.22$ cm downstream of the head end. Because the diffusion flame height is about 110 μm at 70 atm (Cai et al., 2008), the influence of the entropy fluctuation on u' is restricted to the region of the first wavelength of the shear

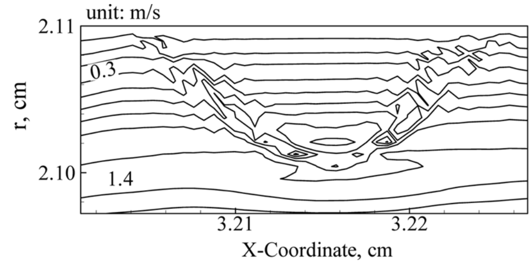

Figure 5 Close-up view of amplitude of axial-velocity fluctuation in flame zone, sandwich propellant located at $x = 3.2$ cm ($f = 1080$ Hz: first longitudinal mode of acoustic oscillation).

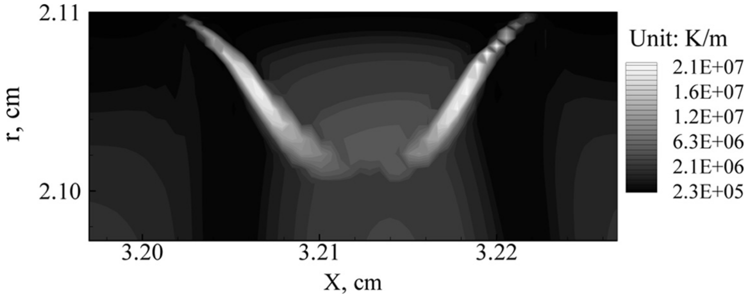

Figure 6 Close-up view of amplitude of temperature-gradient fluctuation, $|(dT/dx)'|$, in flame zone ($f = 1080$ Hz: first longitudinal mode of acoustic oscillation).

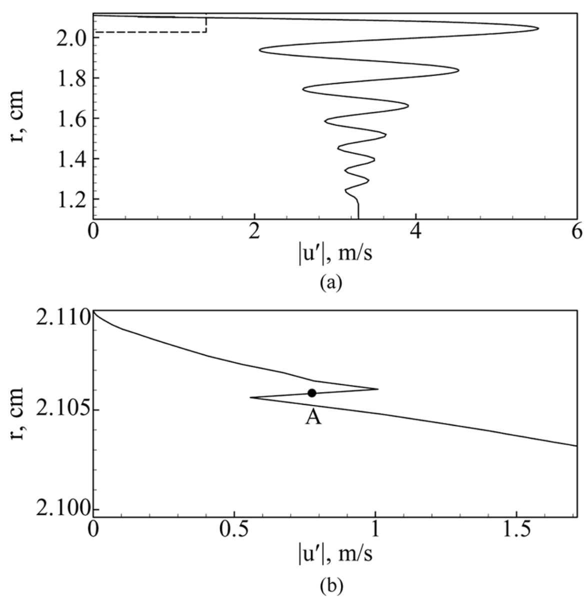

Figure 7 Radial distribution of axial-velocity fluctuation in flame zone; first longitudinal mode of acoustic oscillation ($f = 1080$ Hz): (a) overview (b) close-up view.

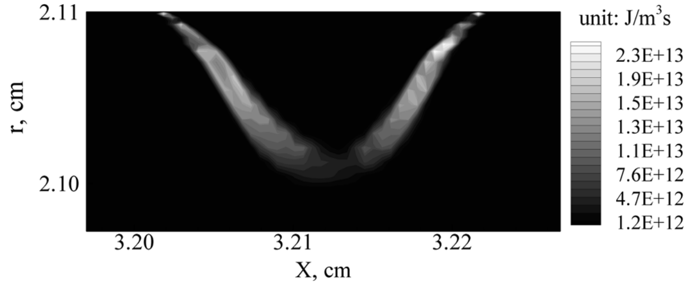

Figure 8 Distribution of amplitude of heat-release fluctuation in flame zone; first longitudinal mode of acoustic oscillation ($f = 1080$ Hz).

wave, as denoted by the dashed line. Figure 7b shows a close-up view. The velocity fluctuation $|u'|$ is distorted on the diffusion flame front (point A). The maximum heat release at the flame front causes a local peak in the temperature distribution, rendering a positive and a negative temperature gradient, $(dT/dx)' > 0$ and $(dT/dx)' < 0$, immediately below and above point A, respectively. The temperature-gradient fluctuation thus exhibits a phase change of π across the flame. The corresponding u'_s shows the same trend, thereby enhancing $|u'|$ on one side and reducing it on the other. The net effect renders a distortion on the oscillating velocity profile, as seen in Figure 7b. Figure 8 shows the distribution of the amplitude of heat-release fluctuation in the flame zone. It bears a close resemblance to those of the velocity and temperature fluctuations in Figures 5 and 6, mainly because the temperature variation is a consequence of the heat-release process.

Figure 9 shows the distribution of entropy fluctuation, $|s'|$, for the first longitudinal mode of acoustic oscillation. The prominence of $|s'|$ even outside the flame zone suggests that the heat-release fluctuation is not the only mechanism producing entropy waves. The temperature fluctuation arising from the mixing between the hot combustion products from the final diffusion flame and the warm fuel pyrolysis species may also play an important role. This phenomenon can be explained based on the following linearized equation of state:

$$s' = C_p \frac{T'}{\overline{T}} - \frac{p'}{\bar{\rho}} \tag{2}$$

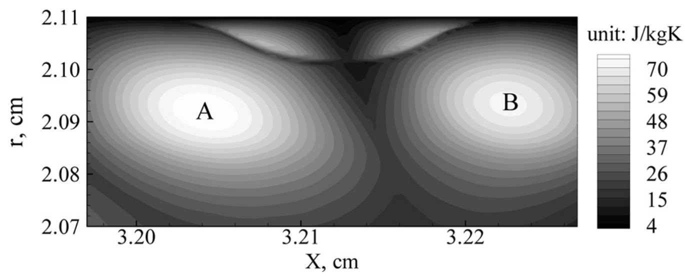

Figure 9 Distribution of amplitude of entropy fluctuation in flame zone; first longitudinal mode of acoustic oscillation ($f = 1080$ Hz).

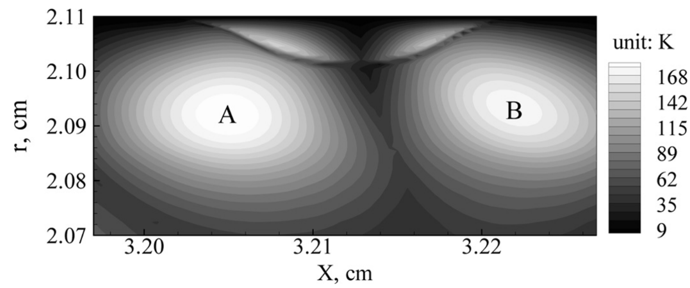

Figure 10 Distribution of amplitude of temperature fluctuation in flame zone; first longitudinal mode of acoustic oscillation ($f = 1080$ Hz).

Figure 10 shows the distribution of temperature fluctuation, $|T'|$. A close correlation between entropy and temperature fluctuations is clearly observed. The maximum $|T'|$ does not occur at the location where the heat release exercises its maximum fluctuation. The situation can be elaborated by considering the temporal evolution of the temperature field. Figure 11 shows the instantaneous temperature distributions at two different times within one cycle of oscillation. The time period of the acoustic oscillation is denoted by τ. As a consequence of acoustic motion, the flamelet moves slightly upstream at $t = 15.25\,\tau$ and then sweeps downstream after one half cycle at $t = 15.75\,\tau$ in response to the local velocity oscillation. This *flame-dancing* phenomenon, along with the ensuing change in the mixing between burned

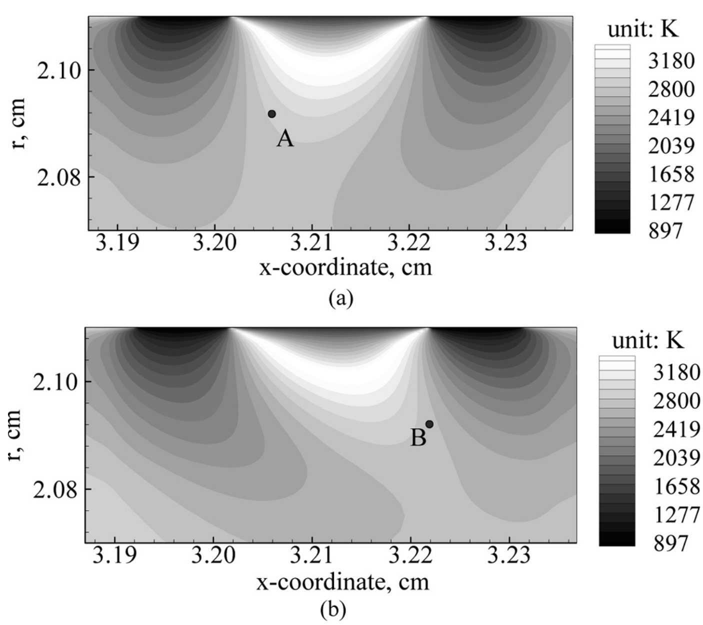

Figure 11 Snapshots of temperature field in flame zone within one cycle of acoustic oscillation, (a) $t = 15.25\ \tau$, (b) $t = 15.75\ \tau$; first longitudinal mode of acoustic oscillation ($f = 1080$ Hz).

products and unburned fuel species outside the flame, is responsible for the formation of the two regimes with intense temperature fluctuation (points A and B in Figure 10). The mutual coupling between the non-uniform flowfield and acoustic oscillations could be as instrumental as the heat-release fluctuation in influencing entropy disturbances.

Vorticity Dynamics

The coupling between acoustic oscillation and combustion response can also be characterized by the following vorticity transport equation:

$$\begin{aligned}\frac{D\Omega}{Dt} = (\Omega \cdot \nabla)\mathbf{u} - \Omega(\nabla \cdot \mathbf{u}) - \nabla(1/\rho) \times \nabla p + \nu\nabla^2\Omega - \mu\nabla(1/\rho) \times (\nabla \times \Omega) \\ + \frac{4}{3}\mu(1/\rho) \times \nabla(\nabla \cdot \mathbf{u})\end{aligned} \tag{3}$$

where Ω is the vorticity defined as $\nabla \times \mathbf{u}$. In the case without heat release, vorticity is produced at the wall to satisfy the non-slip condition. In the present case, the heat release in the flame zone gives rise to non-uniform distributions of density, pressure, and temperature. Vorticity can thus be produced through baroclinicity and volume dilatation, represented by $-\nabla(1/\rho) \times \nabla p$ and $-\Omega(\nabla \cdot \mathbf{u})$, respectively. The resultant vorticity enhances the fuel/oxidizer mixing and subsequently modifies the characteristics of the diffusion flame above the burning propellant.

The acoustic-wave-induced vorticity generation and transport in a cold-flow environment has been elaborated by Flandro (1995) and Majdalani and Roh (2000) for laminar flows, as well as by Flandro et al. (2000) and Apte and Yang (2002) for turbulent flows. The focus of the present study is on the vorticity evolution caused by the interactions between acoustic oscillations and propellant combustion. The perturbed baroclinicity term has two components: $\nabla(1/\bar{\rho}) \times \nabla p'$ and $\nabla(1/\rho') \times \nabla\bar{p}$. The former results from the coupling between the acoustic-pressure and time-averaged flowfields. The latter is attributed to the heat-release fluctuation in the flame zone. The perturbed volume-dilatation term includes two components: $\overline{\Omega}(\nabla \cdot \mathbf{u}')$ and $\Omega'(\nabla \cdot \mathbf{u})$, accounting for the compressibility effect. Figures 12a and 12b show snapshots of fluctuating vorticity at the downstream end of the motor within one cycle of acoustic oscillation, corresponding to the two extremes of the flame-tip locations. The unsteady flame is accompanied by a pair of opposite vortices on the two sides of the flame front. The temperature gradients at these locations also exhibit opposite signs. Because the pressure gradient associated with the flame is not significant, the density field is dictated by the local temperature variation. Opposite vortices are thus generated on the two sides of the flamelet through the baroclinicity mechanism. As the acoustic pressure gradient changes its sign from $15.25\,\tau$ to $15.75\,\tau$, the corresponding unsteady vortices also alter their directions. At a given time instant, however, the vortices on the two sides retain opposite signs. Figure 13 illustrates the acoustic-oscillation-induced vorticity fluctuation. Such vortices provide an additional mechanism to enhance the mixing between the fuel and oxidizer streams and consequently the diffusion-controlled reaction. The flamelet is dragged closer to the propellant surface. The resultant elevation of heat feedback increases

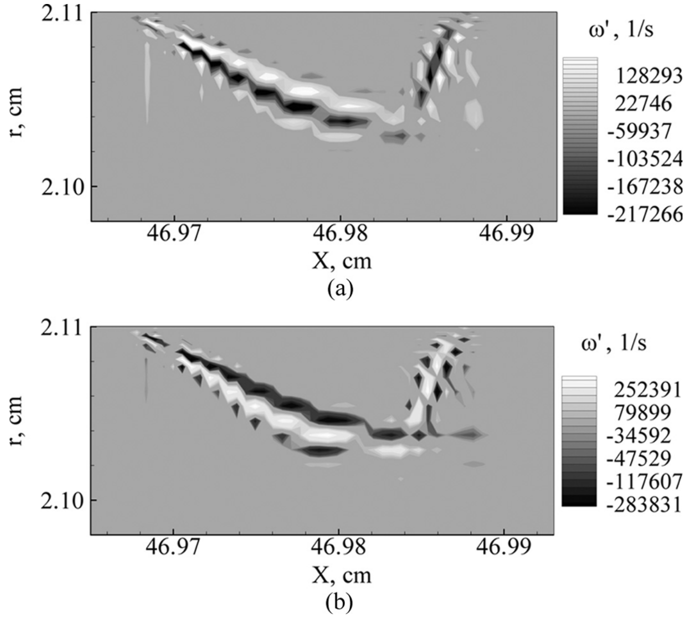

Figure 12 Snapshots of fluctuating vorticity field for a sandwich propellant located at downstream end ($x/\mathrm{L} = 0.94$) within one cycle of acoustic oscillation, (a) $t = 15.25\,\tau$ (b) $t = 15.75\,\tau$; first longitudinal mode of acoustic oscillation ($f = 1080$ Hz).

the propellant burning rate. Figure 14 shows the time evolution of the temperature gradient and mass flux at the propellant surface. The influence of vorticity fluctuation on the propellant burning behavior is clearly observed. Such enhancement of diffusive combustion due to vortices was also noted by Marble (1985).

Rayleigh's Criterion

The correlation between unsteady heat release and acoustic pressure fluctuation provides a quantitative measure of the extent to which the flame may drive or suppress the flow oscillations. This is achieved by calculating the Rayleigh parameter, $\langle p'q' \rangle$, a time-averaged quantity of the product of acoustic and heat-release fluctuations over one cycle of oscillation. An acoustic wave can be excited or damped

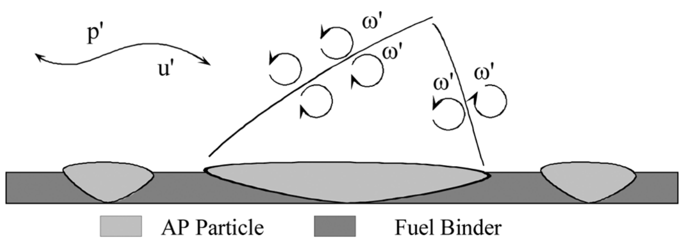

Figure 13 Schematic diagram illustrating acoustically induced vorticity fluctuation.

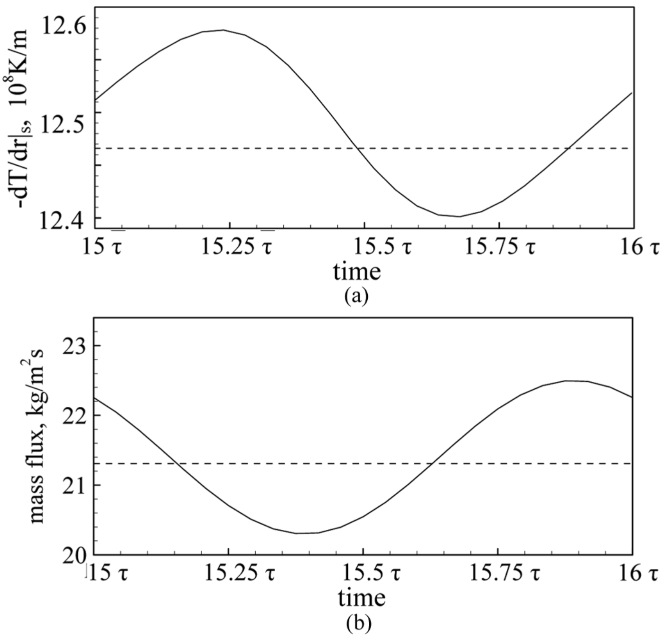

Figure 14 Time evolution of (a) temperature gradient and (b) mass flux at propellant surface, showing influence of vorticity on propellant burning behavior (----- steady-state condition).

if the integral is positive or negative, respectively. Figure 15 shows the Rayleigh parameter for the first two modes of acoustic oscillation near the chamber head-end. The parameter exhibits both positive and negative peaks with about the same magnitude in the flame zone. Similar to the situation for a premixed flame in homogenous propellant combustion (Roh et al., 1998), the diffusion flame serves as an acoustic

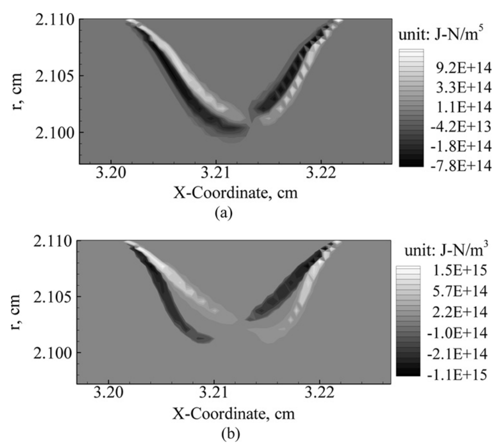

Figure 15 Distribution of Rayleigh's parameter near the chamber head-end (a) first mode ($f = 1080\,\text{Hz}$) and (b) second mode ($f = 2160\,\text{Hz}$)

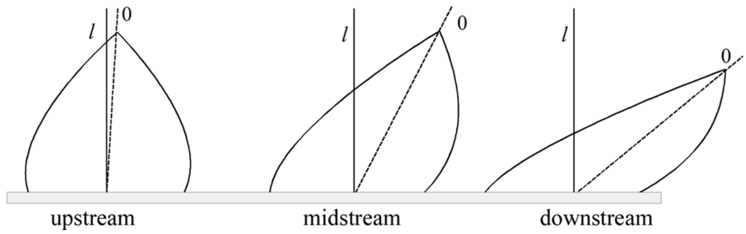

Figure 16 Flame shapes at different chamber locations in presence of crossflow at steady-state.

dipole source. For the second mode, the flamelet oscillates over a wider spatial range, due to the longer perturbation of the axial flow in the flame zone.

Propellant Combustion Response

The presence of crossflow increases the heat transfer to the propellant by bending the flame towards the surface (Cai et al., 2008). Figure 16 shows schematically the situation at various locations in the chamber under a steady-state condition. The dashed line 0 corresponds to the flame centerline, denoting the flame orientation, whereas the solid line *l* serves as a reference coordinate perpendicular to the propellant surface. The flame tilts more severely in the downstream region, where the crossflow is stronger. In the case of acoustic excitation, the flame oscillates in response to local flow variations of pressure and velocity, thereby modifying the heat feedback to the surface and subsequently the propellant burning rate. Figure 17 illustrates the flame dynamics at three different chamber locations under the influence of acoustic excitation. The solid and dashed lines, 0 and *l*, correspond to those in Figure 16 at steady-state. Lines 1 and 2 represent the two extreme locations of the flame centerline as it fluctuates back and forth during one acoustic cycle. Depending on the location of the propellant segment, two different scenarios exist for the energy-feedback fluctuation. The first scenario pertains to regions where $|u'|$ is so small that the flame centerline oscillates only downstream of the vertical line *l*, such as regions neighboring the acoustic velocity node points (e.g., locations 1 and 3 in Figure 2a). The energy feedback to the propellant surface increases monotonically as the flame moves closer to the propellant surface from line 1 to 2 in the first half cycle of oscillation, and decreases monotonically in the second half cycle when the path is reversed. This yields a maximum and a minimum value of the energy feedback at lines 2 and 1, respectively. The second scenario pertains to regions where

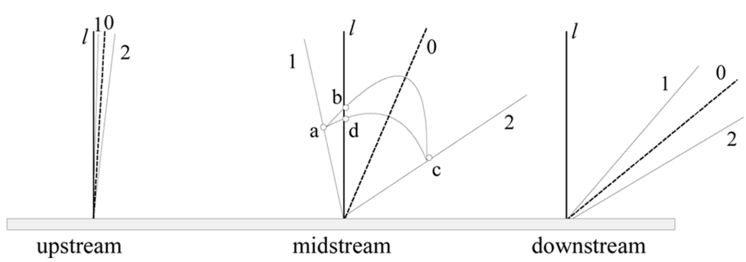

Figure 17 Flame shapes at different chamber locations in presence of crossflow under acoustic oscillation.

$|u'|$ is sufficiently large to cause the flame centerline to oscillate across line *l*, as in regions near the acoustic velocity anti-node points (e.g., location 2 in Figure 2a for the first longitudinal mode). During the first half cycle of oscillation, the flame moves away from the propellant surface from *a* to *b*, leading to a decrease in the energy feedback to the propellant. As time proceeds, the flame begins to move closer to the surface from *b* to *c*, and the heat transfer to the propellant is elevated. In the second half cycle, the entire trend is reversed. Therefore, in the case of the first longitudinal mode of the standing acoustic wave at the midstream location, the energy feedback to the propellant within one cycle of oscillation exhibits two peak values at, *a* and *c*, and two minimum values, at *b* and *d*.

In the context of the above analysis, Figure 18 shows the response of the propellant-surface heat transfer to the pressure and velocity fluctuations for the first

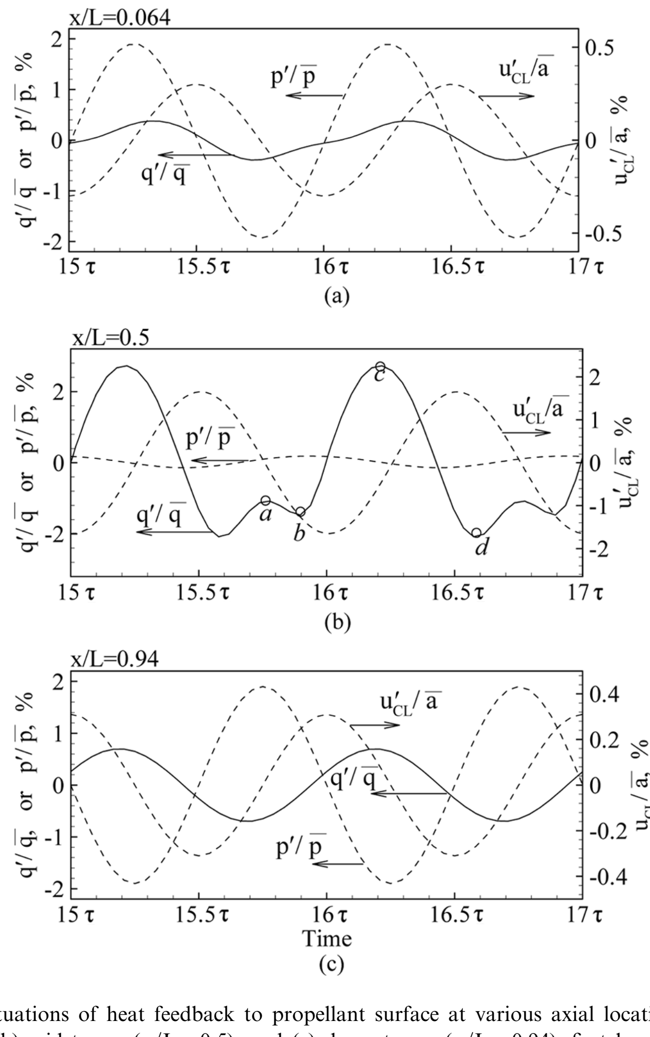

Figure 18 Fluctuations of heat feedback to propellant surface at various axial locations (a) upstream ($x/\mathrm{L} = 0.064$), (b) midstream ($x/\mathrm{L} = 0.5$), and (c) downstream ($x/\mathrm{L} = 0.94$); first longitudinal mode of acoustic oscillation ($f = 1080$ Hz).

longitudinal mode of the standing acoustic wave. The results for three different chamber locations are presented. The axial-velocity fluctuation at the centerline of the chamber serves as an indication of the magnitude of crossflow oscillation. The heat flux to the propellant surface is calculated by taking a spatial average over the entire surface, given by

$$\dot{q} = \frac{1}{S}\int_S \left(-\lambda \frac{dT}{dr}|_{y=R}\right) ds \tag{4}$$

The strong velocity fluctuation at the midstream location (i.e., the acoustic velocity anti-node point) leads to two local maxima and two minima in the heat-flux oscillation within one cycle of acoustic excitation. The corresponding amplitude at the chamber head-end and exit (i.e., acoustic velocity node), however, exhibits a single maximum and a minimum. The magnitude of oscillation is much smaller than that of the midstream location. This suggests the dominance of velocity fluctuation over pressure fluctuation in controlling the heat feedback from the flame to the propellant surface.

The situation is substantially changed for the second mode of wave motion due to the different spatial distribution of $|u'|$, as shown in Figure 19. In the chamber upstream region, the amplitude of the velocity fluctuation exceeds its time-mean value, causing the flame centerline to oscillate across line l. The phenomenon bears a close resemblance to that at the midstream location for the first mode of acoustic

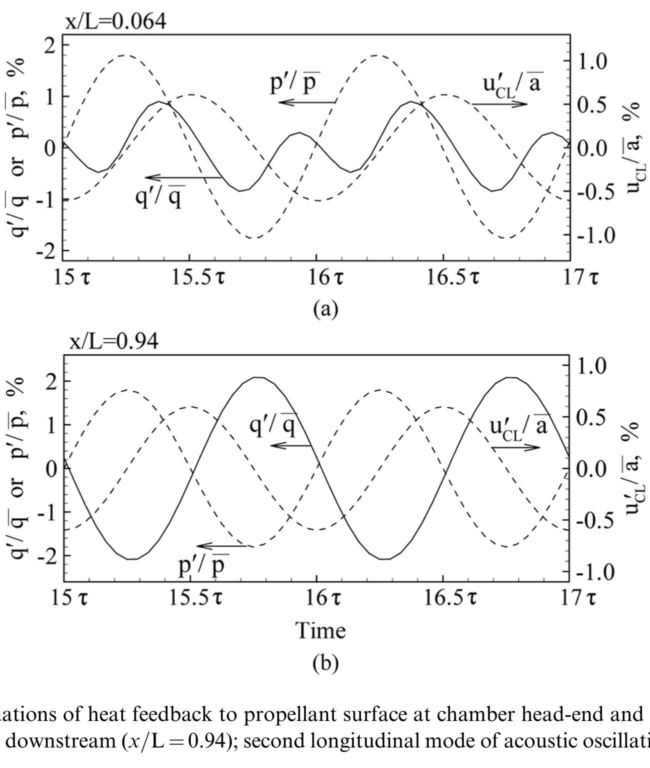

Figure 19 Fluctuations of heat feedback to propellant surface at chamber head-end and exit (a) upstream ($x/\mathrm{L} = 0.064$) (b) downstream ($x/\mathrm{L} = 0.94$); second longitudinal mode of acoustic oscillation ($f = 2160$ Hz).

oscillation (see Figure 18b). At the downstream end, the time-mean crossflow velocity overrides its fluctuating counterpart, thereby eliminating the velocity modulation effect. The propellant-surface heat flux varies sinusoidally with a much higher amplitude, in response to the local flow oscillation. For the same velocity fluctuation, the stronger crossflow in the downstream region tends to enhance the propellant combustion response due to the flame-bending effect.

Figure 20 shows the time evolution of the propellant burning rate near the chamber head-end ($x/\mathrm{L} = 0.064$) for the first three modes of longitudinal acoustic oscillation. For the first mode, the velocity fluctuation is small and the propellant mass burning-rate fluctuation, $\dot{m}'$, is mainly induced by the acoustic pressure. The combustion response function, defined as $R_p = (\dot{m}'/\bar{\dot{m}})/(p'/\bar{p})$, only has a real part of 0.94, indicating a strong correlation with the pressure oscillation. The velocity

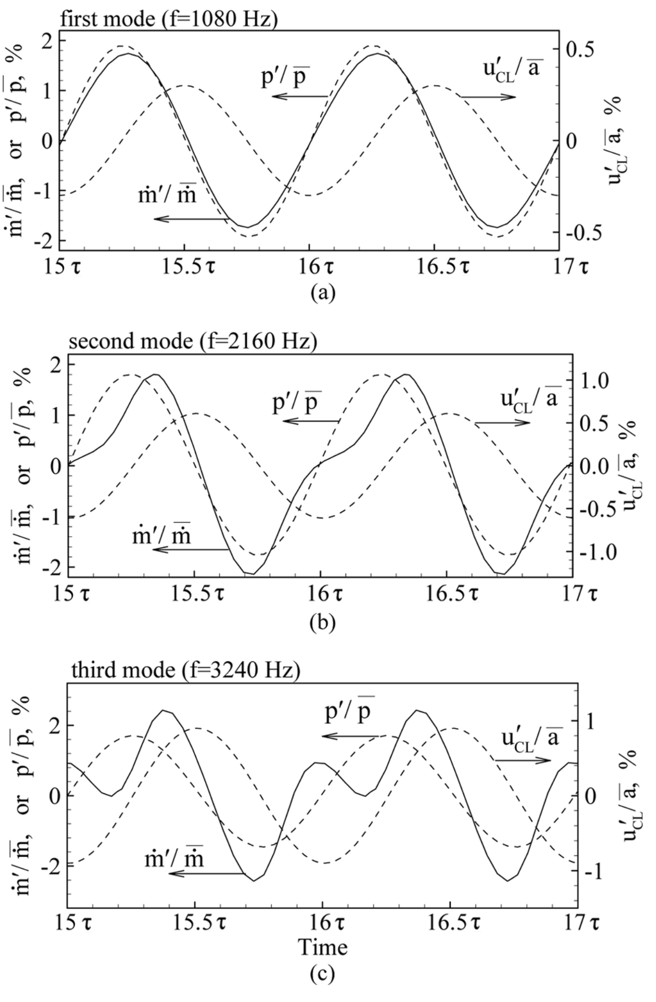

Figure 20 Fluctuation of propellant mass burning rate near chamber head-end ($x/\mathrm{L} = 0.064$ m), (a) first mode ($f = 1080$ Hz), (b) second mode ($f = 2160$ Hz), and (c) third mode ($f = 3240$ Hz).

fluctuation increases progressively from the first to the third mode, as shown in Figure 2, and a similar trend is observed in the corresponding values of $\dot{m}'$. A Fourier analysis on $\dot{m}'$ for the third mode shows two dominant frequencies of 3240 and 6480 Hz, which correspond to the first and second harmonic of the imposed oscillation. Although the acoustic excitation has a single frequency, the resultant burning-rate fluctuation features higher harmonics. Such a non-linear behavior can be attributed to the velocity-modulation phenomenon and the occurrence of multiple peaks in the ensuing heat-flux fluctuation at the propellant surface.

Figure 21 shows the burning-rate response to the first mode of acoustic oscillation at three different axial locations. At the chamber midstream location where the highest velocity fluctuation occurs, the burning-rate oscillation exhibits higher harmonics. In contrast, only a single sinusoidal variation is present near the chamber head-end and exit because of the low level of velocity fluctuation. It has often been

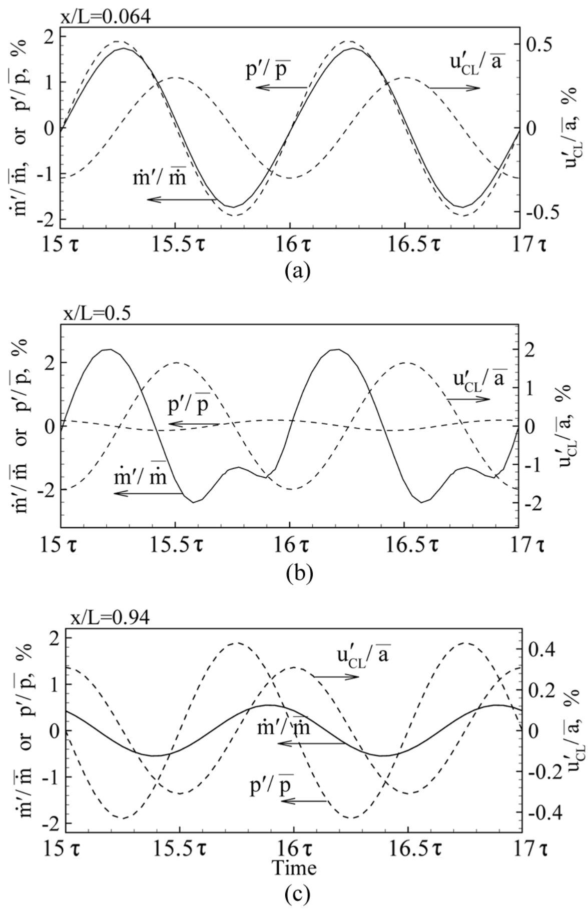

Figure 21 Fluctuations of mass burning rate at various axial locations for first longitudinal mode of acoustic oscillation ($f = 1080$ Hz), (a) upstream ($x/\mathrm{L} = 0.064$), (b) midstream ($x/\mathrm{L} = 0.5$), and (c) downstream ($x/\mathrm{L} = 0.94$).

observed for AP/HTPB composite propellants that the combustion response to a single-frequency excitation features multiple harmonics. This phenomenon may arise from the modulation of the flow velocity above the propellant surface, particularly because of the reversal in the local flow direction due to acoustic oscillation. It is possible that the multi-modal distribution of AP particle size also contributes to this nonlinear behavior, but this notion is not well-established quantitatively and is still under scrutiny.

The velocity-coupled combustion response manifests itself through both the oscillatory and mean crossflows. The difference observed in the burning-rate fluctuation between Figures 21a and 21c, despite the equal magnitudes of pressure and velocity oscillations at these two locations, indicates the significance of the time-averaged crossflow. At the chamber head-end, the response function R_p has a real part of 0.94. Its imaginary part is negligibly small. At the downstream location, however, R_p has a real and an imaginary part of 0.34 and -0.41, respectively. The disparity of the combustion response in both the magnitude and phase indicates that mean-flow convection also plays a decisive role in determining the propellant combustion dynamics.

Thermal Wave in Condensed Phase

The interaction between the acoustic oscillation and the gas-phase flame dynamics causes a temperature fluctuation at the propellant surface. A thermal wave thus propagates into the condensed phase through the diffusion process. Figure 22 shows the magnitude of temperature fluctuation and time-averaged temperature in the condensed phase at the chamber head-end for the first longitudinal mode of acoustic excitation. The penetration depth (δ_c) of the thermal wave associated with acoustic forcing is less than 2 μm into the reactive-diffusive zone, leaving the bulk of the preheat zone unaffected. Such a small value is attributed to the large thermal inertia (inversely proportional to thermal diffusivity, α) of the condensed phase. A simple dimensional analysis gives $\delta_C \sim \sqrt{\alpha/f}$, indicating a decrease in δ_c with increasing acoustic frequency f. Figure 23 shows the amplitude of temperature

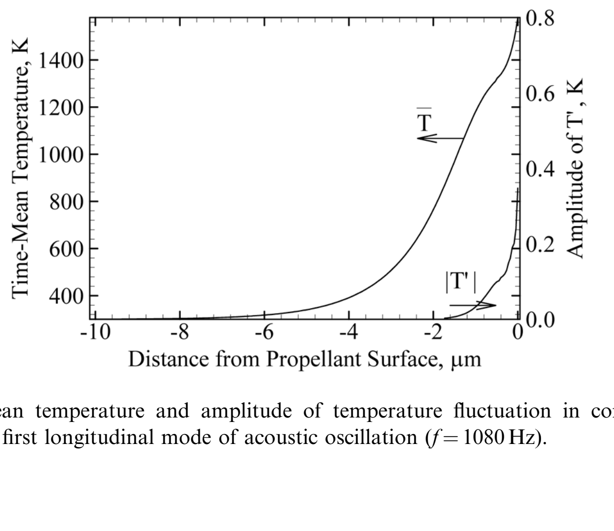

Figure 22 Time-mean temperature and amplitude of temperature fluctuation in condensed phase at chamber head-end; first longitudinal mode of acoustic oscillation ($f = 1080$ Hz).

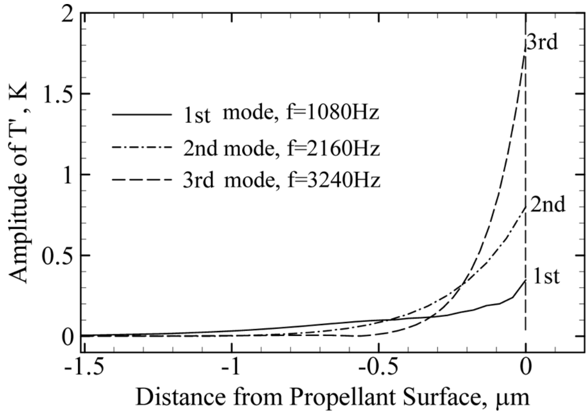

Figure 23 Amplitudes of temperature fluctuations in condensed phase at chamber head-end for first three modes of acoustic oscillation.

fluctuation at the chamber head-end for the first three longitudinal modes of acoustic excitation. The maximum surface temperature fluctuations $|T'_S|$ are 0.3, 0.8, and 1.8 K for the three modes, respectively. The penetration depth decreases from the first to the third mode, which is consistent with the result from the aforementioned dimensional analysis.

CONCLUSIONS

The transient combustion response of AP/HTPB propellant to standing acoustic oscillations in a rocket-motor environment has been studied. Emphasis was placed on the near-surface flame-zone physiochemistry and propellant combustion response. The situations in various parts of the chamber were explored for the first three modes of acoustic excitation. The interactions between the flame dynamics and acoustic excitations, as well as the ensuing influence on the propellant burning behavior, were studied by examining the contributions of the acoustic, vorticity, and entropy modes of disturbances to the oscillatory flowfield. The entropy disturbance is mainly associated with the temperature fluctuation arising from the nonuniform heat release in the flame zone under acoustic excitation. Unsteady vortices with opposite orientations are generated on the different sides of the diffusion flame front. These vortices tend to enhance the mixing between the fuel and oxidizer streams in the gas phase and consequently elevate the propellant burning rate. The oscillatory diffusion flame serves as an acoustic dipole source driving flow instability in the chamber. The velocity-induced combustion response caused by the crossflow oscillation may overshadow the pressure-coupled response, depending on the propellant location, acoustic forcing frequency and amplitude, and mean flow properties. In addition, a single-frequency excitation may lead to multiple harmonics in the propellant combustion response. This non-linear phenomenon can be attributed to the modulation of the flow speed and direction by the acoustic oscillation in the flame zone. The mean-flow convection also plays an important role in determining the propellant combustion response through its influence on the flame structure.

NOMENCLATURE

a	speed of sound
f	frequency
$\dot{m}$	mass burning rate of propellant
p	pressure
q	heat-release rate
$\dot{q}$	heat flux to propellant surface
r	radial coordinate
R	radius of rocket motor
R_p	combustion response function
s	entropy
T	temperature
t	time
u, v	velocity components in axial and radial coordinates, respectively
x	axial coordinate

Greek Symbols

α	thermal diffusivity
δ	penetration depth of thermal wave
ρ	density
Ω	vorticity
τ	period of acoustic oscillation

Subscripts

a	acoustic mode
c	condensed phase
s	surface quantity or entropy mode
v	vorticity mode

Superscripts

$'$	fluctuating quantity
—	time-averaged quantity

REFERENCES

Apte, S., and Yang, V. 2002. Unsteady flow evolution in porous chamber with surface mass injection, Part 2: Acoustic excitation. *AIAA Journal*, **40**, 244.

Baum, J.D., and Levine, J.N. 1986. Modeling of nonlinear longitudinal instability in solid rocket motors. *Acta Astronautica*, **13**, 339.

Brewster, M.Q., and Son, S.F. 1995. Quasi-steady combustion modeling of homogeneous solid propellants. *Combustion and Flame*, **103**, 11.

Brewster, M.Q., Ward, M.J., and Son, S.F. 2000. Quasi-steady combustion modeling of homogeneous solid propellants. *Combustion Science and Tech.*, **154**, 1.

Cai, W., Ma, F.H., and Yang, V. 2003. Two-phase flow interactions in solid-propellant rocket motors with acoustic oscillations. *Journal of Propulsion and Power*, **19**, 385.

Cai, W., Thakre, P., and Yang, V. 2008. A model of AP/HTPB composite propellant combustion in rocket motor environments. *Combustion Science and Tech.*, **180**, 2143.

Chu, W.-W., Yang, V., and Majdalani, J. 2003. Premixed flame response to acoustic waves in a porous-walled chamber with surface mass injection. *Combustion and Flame*, **133**, 359.

Cohen, N.S., and Strand, L.D. 1985a. Combustion response to compositional fluctuations. *AIAA Journal*, **23**, 760.

Cohen, N.S., and Strand, L.D. 1985b. Effects of AP particle size on combustion response to cross flow. *AIAA Journal*, **23**, 776.

Culick, F.E.C. 1968. A review of calculations for unsteady burning of a solid propellant. *AIAA Journal*, **6**, 2241.

Culick, F.E.C., and Yang, V. 1992. Prediction of the stability of unsteady motions in solid propellant rocket motors. In De Luca, L., Price, E.W., and Summerfield, M. (Eds.), *Nonsteady burning and combustion stability of solid propellants*, vol. 143. Progress in Astronautics and Aeronautics, AIAA, 719, Washington, DC.

Flandro, G.A. 1995. Effects of vorticity on rocket combustion stability. *Journal of Propulsion and Power*, **11**, 607.

Flandro, G.A., Cai, W., and Yang, V. 2000. Turbulent transport in rocket motor unsteady flowfield. In Yang, V., Brill, T.B., and Ren, W.Z. (Eds.), *Solid propellant chemistry, combustion and motor interior ballistics*, vol. 185. Progress in Astronautics and Aeronautics, AIAA, 837, New York.

Guirao, C., and Williams, F.A. 1971. A model for aluminum perchlorate deflagration between 20 and 100 atm. *AIAA Journal*, **9**, 1345.

Hsieh, S.Y., and Yang, V. 1997. A preconditioned flux-differencing scheme for chemically reacting flows at all mach numbers. *J. Comp. Fluid Dyn.,* **8**, 31.

Levine, J.N., and Baum, J.D. 1983. Numerical study of nonlinear instability phenomenon in solid rocket motors. *AIAA Journal*, **21**, 557.

Majdalani, J. 1999. The boundary layer structure in cylindrical rocket motors. *AIAA Journal*, **37**, 505.

Majdalani, J., and Roh, T.S. 2000. The oscillatory channel flow with large wall injection. *Proceedings of the Royal Society, London, Series A*, **456**, 1625.

Majdalani, J., and Van Moorhem, W.K. 1997. A multiple-scales solution to the acoustic boundary layer in solid rocket motors. *Journal of Propulsion and Power*, **13**, 186.

Marble, F.E. 1985. Growth of a diffusion flame in the field of a vortex. In Casci, C. (Ed.), *Recent advances in the aerospace science – In honor of Luigi Crocco on his seventy-fifth birthday*, Plenum Prenum, New York, pp. 395–414.

Novozhilov, B.V. 1965. Burning of a powder under harmonically varying pressure. *Journal of Appl. Mech. Tech. Phys.*, **6**, 103.

Pierce, A.D. 1989. *Acoustics: An introduction to its physical principles and applications*. The Acoustical Society of America, New York.

Roh, T.S., Apte, S.V., and Yang, V. 1998. Transient combustion response of homogeneous solid propellant to acoustic oscillations in a rocket motor. *Proceedings of the Combustion Institute,* **27**, 1381.

Tseng, L.S., and Yang, V. 1994. Combustion of a double-base homogeneous propellant in a rocket motor. *Combustion and Flame*, **96**, 325.

Wicker, J.M., Greene, W.D., Kim, S.-I., and Yang, V. 1996. Triggering of longitudinal combustion instabilities in rocket motors: Nonlinear combustion response. *Journal of Propulsion and Power*, **12**, 1148.

Zong, N., and Yang, V. 2007. An efficient preconditioning scheme for general fluid mixtures using primitive pressure-temperature variables. *International Journal of Computational Fluid Dynamics*, **21**, 217.

Zong, N., and Yang, V. 2008. Cryogenic fluid dynamics of pressure swirl injectors at supercritical conditions. *Physics of Fluids*, **20**, 056103.